

Supplementary Material

Piezoelectric cellulose/poly(vinylidene fluoride) glycerogels with synergistically enhanced energy output for wide temperature range

Md. Tariful Islam Mredha^{1,#}, Rumesh Rangana Manimel Wadu^{1,#}, Shuangpeng Li^{2,3,#}, Adith Varma Rama Varma¹, Tanish Gupta¹, Wonoh Lee¹, Chunli Zhang^{2,3,*}, Weiqiu Chen^{2,3,*}, Insu Jeon^{1,*}

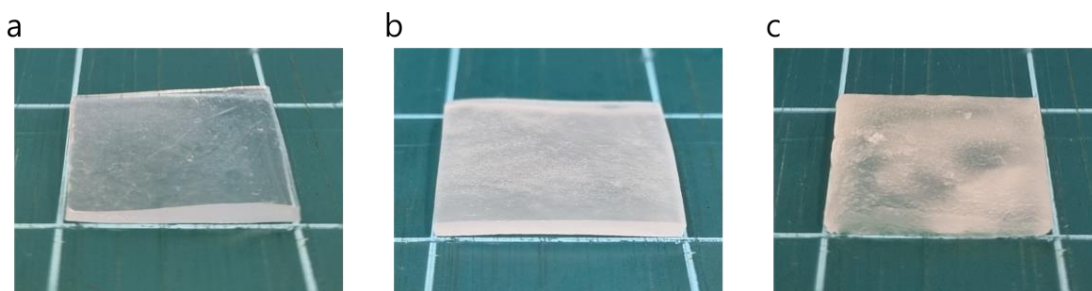
¹School of Mechanical Engineering, Chonnam National University, Gwangju 61186, Republic of Korea.

²Key Laboratory of Soft Machines and Smart Devices of Zhejiang Province, Department of Engineering Mechanics, Zhejiang University, Hangzhou 310027, Zhejiang, China.

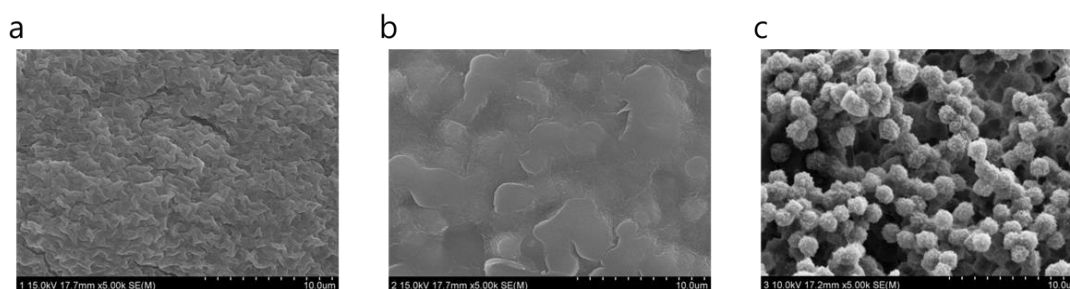
³Huanjiang Laboratory, Zhuji 311816, Zhejiang, China.

#Authors contributed equally.

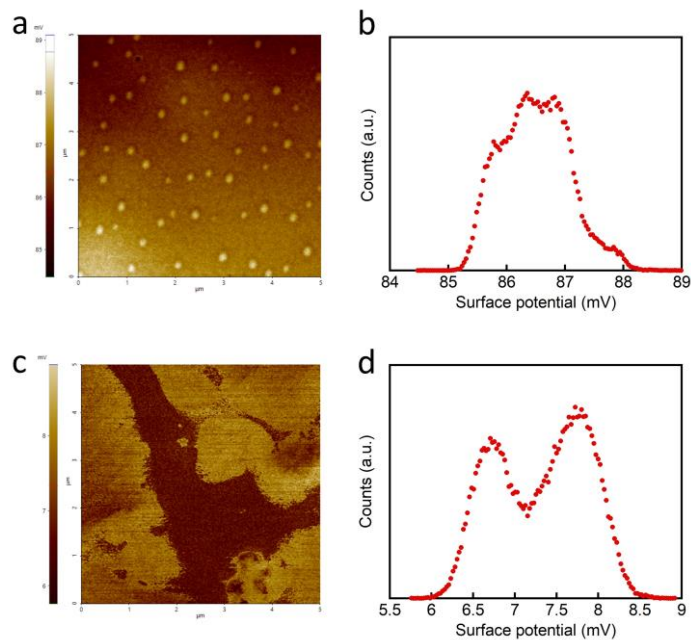
Correspondence to: Dr. Chunli Zhang, Key Laboratory of Soft Machines and Smart Devices of Zhejiang Province, Department of Engineering Mechanics, Zhejiang University, Hangzhou 310027, Zhejiang, China; Huanjiang Laboratory, Zhuji 311816, Zhejiang, China. E-mail: zhangcl01@zju.edu.cn; Dr. Weiqiu Chen, Key Laboratory of Soft Machines and Smart Devices of Zhejiang Province, Department of Engineering Mechanics, Zhejiang University, Hangzhou 310027, Zhejiang, China; Huanjiang Laboratory, Zhuji 311816, Zhejiang, China. E-mail: chenwq@zju.edu.cn; Dr. Insu Jeon, School of Mechanical Engineering, Chonnam National University, 77 Yongbong-ro, Buk-gu, Gwangju 61186, Republic of Korea. E-mail: i_jeon@chonnam.ac.kr



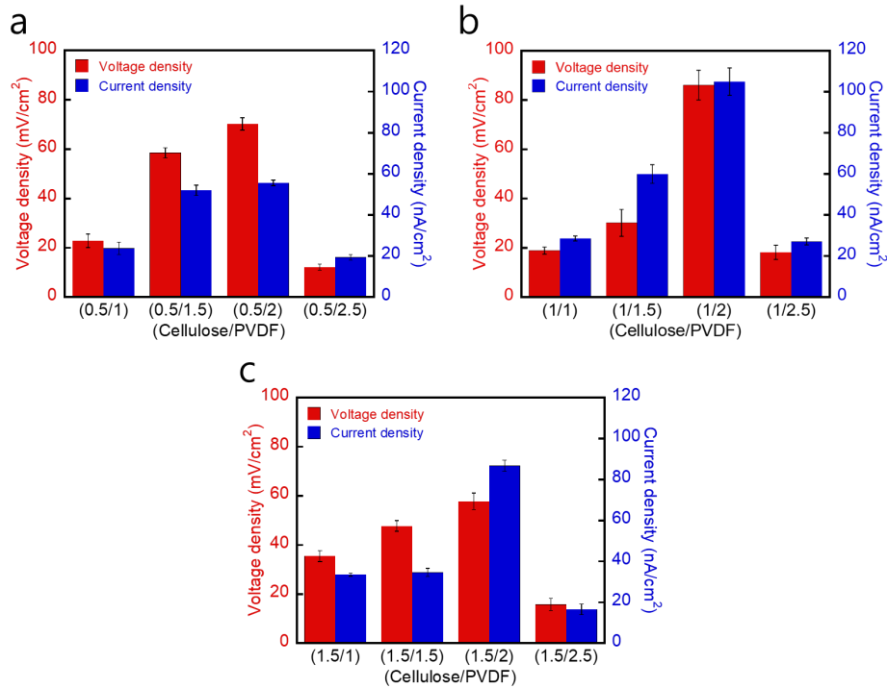
Supplementary Figure 1. Photographs of the prepared GGs: (a) 1% cellulose, (b) (1/2)% cellulose/PVDF, and (c) (0.5/5)% cellulose/PVDF.



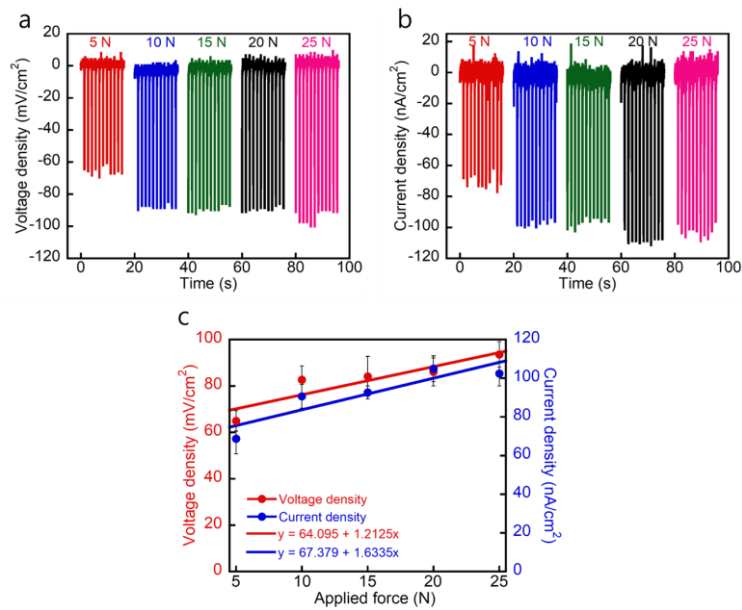
Supplementary Figure 2. Field-emission scanning electron microscopy (FE-SEM) images of hydrogels: (a) 1% cellulose, (b) (1/2)% cellulose/PVDF, and (c) (0.5/5)% cellulose/PVDF.



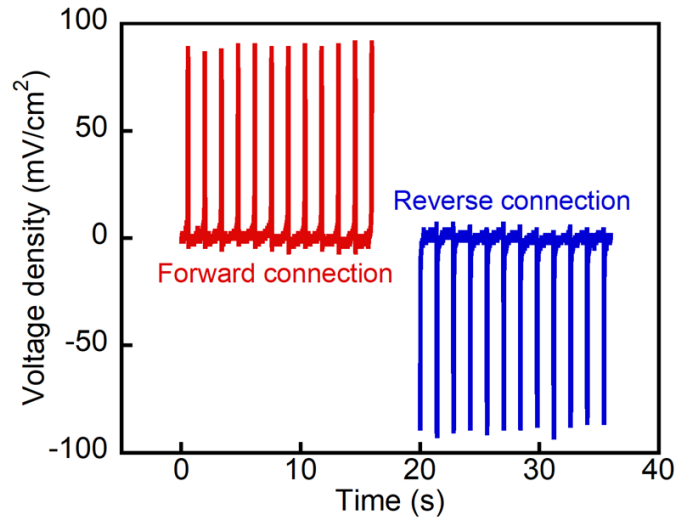
Supplementary Figure 3. Surface potential distribution images (left) and their corresponding distribution curves (right) of (a, b) (1/2)% cellulose/PVDF GG (c, d) and 1% cellulose GG.



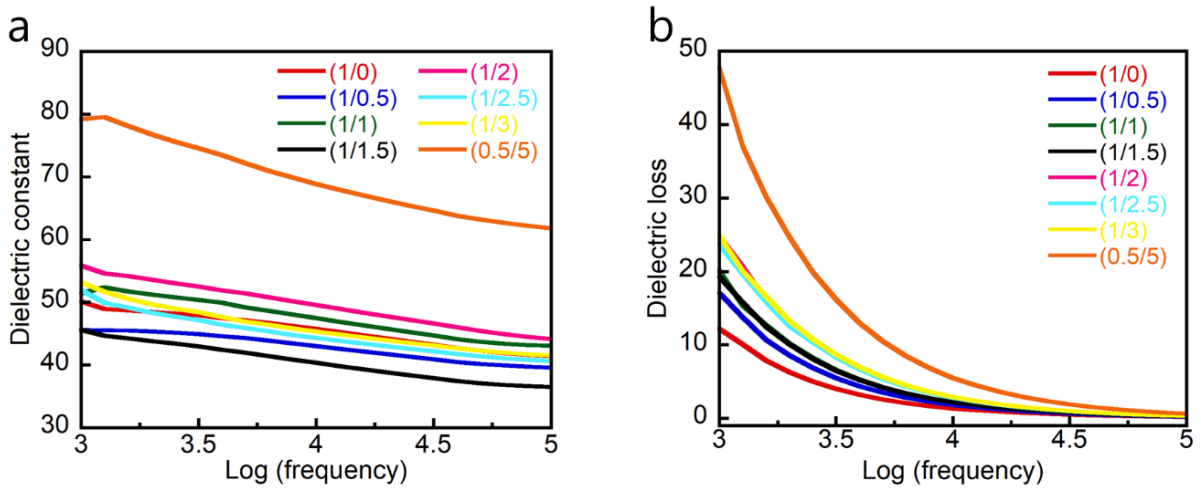
Supplementary Figure 4. Piezoelectric output voltages and current densities of cellulose/PVDF GGs with three different cellulose concentrations: (a) 0.5%, (b) 1%, and (c) 1.5%.



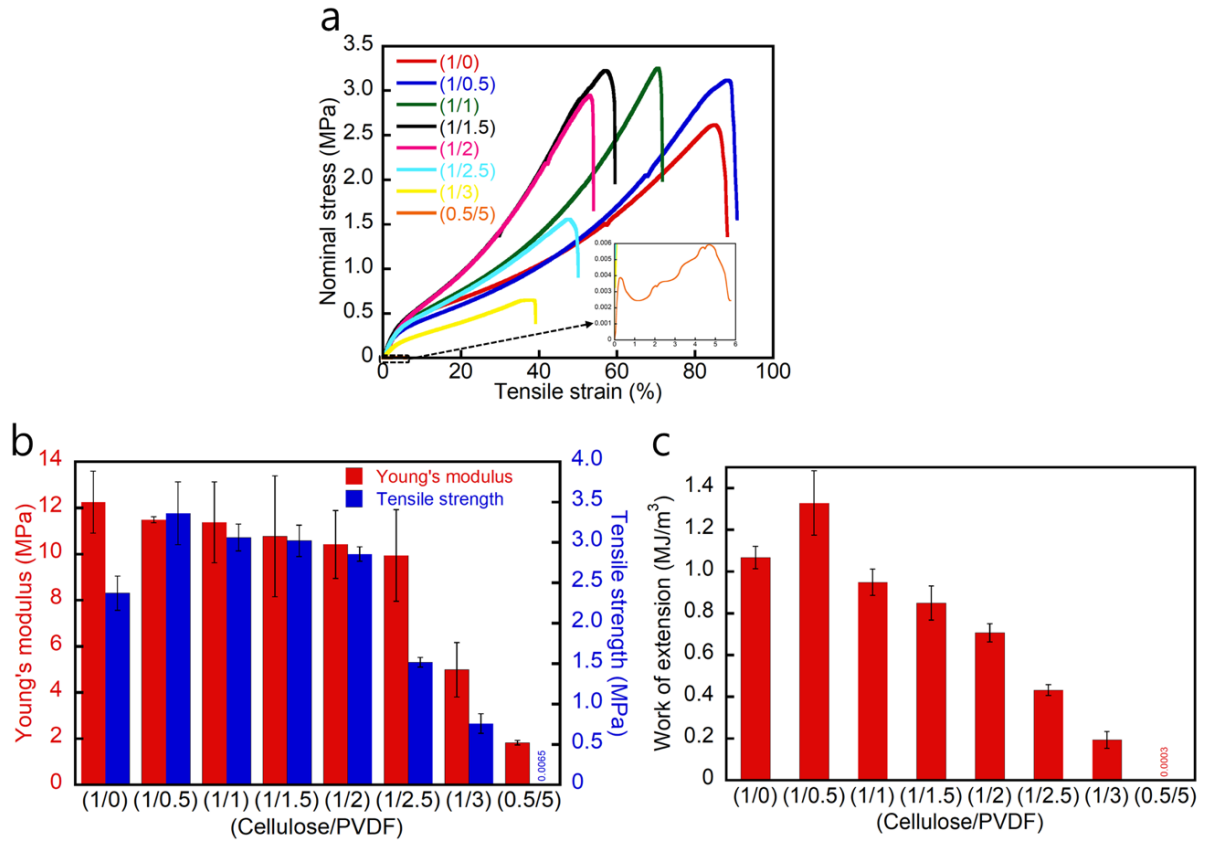
Supplementary Figure 5. Mechanical–electrical response characteristics of (1/2)% cellulose/PVDF GG under different loads: (a) output voltage density and (b) output current density measured with respect to time under various applied loads. (c) Output voltage and current density as functions of the applied force, which ranged between 5 and 25 N owing to machine limitations.



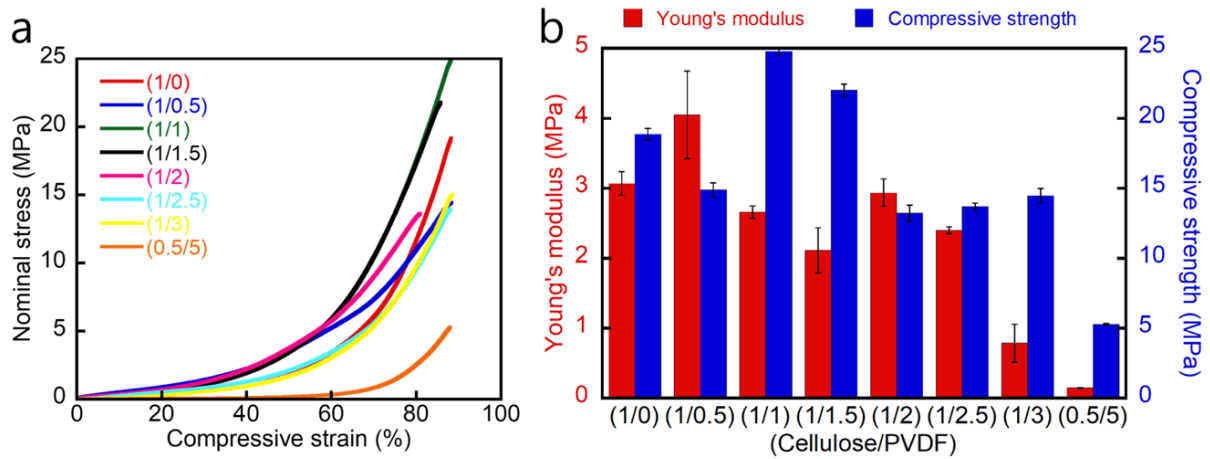
Supplementary Figure 6. Voltage output of (1/2)% cellulose/PVDF GG under a constant force of 20 N with forward and reverse connections.



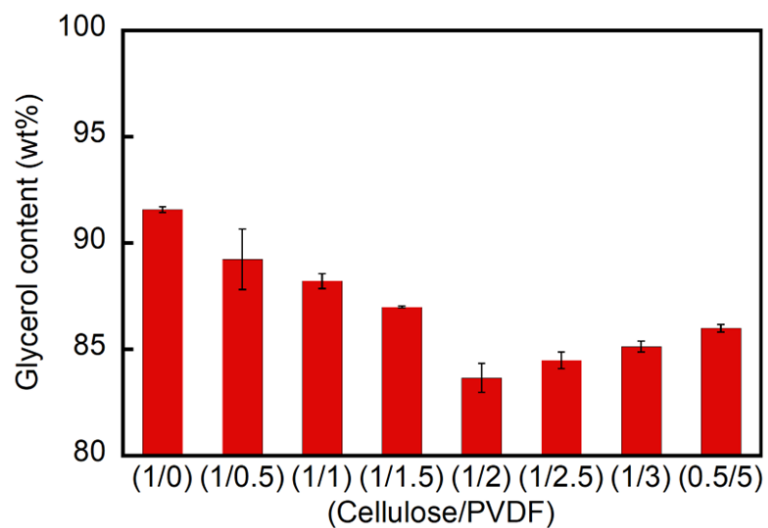
Supplementary Figure 7. Dielectric properties of various cellulose/PVDF GGs as functions of the log(frequency): (a) dielectric constant and (b) dielectric loss.



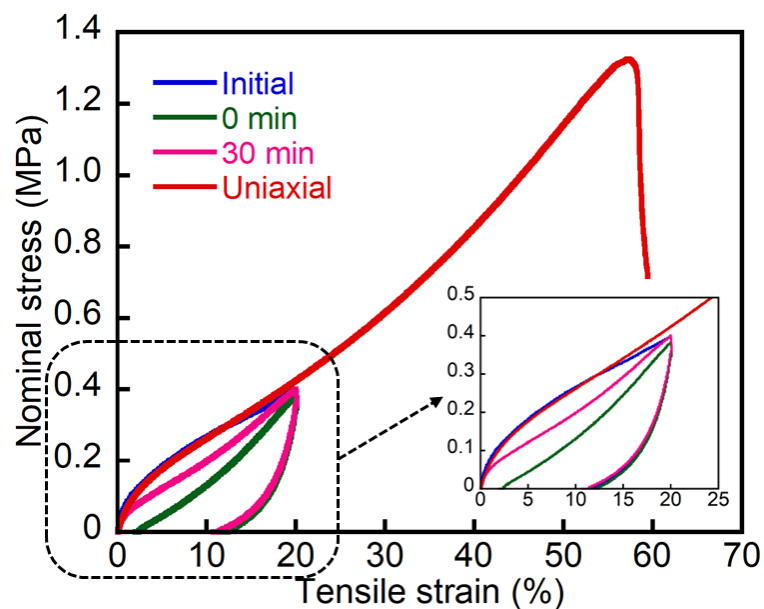
Supplementary Figure 8. (a) Tensile stress–strain curves of the cellulose/PVDF GGs, (b) corresponding Young’s moduli (left) and tensile strengths (right), and (c) work of extension.



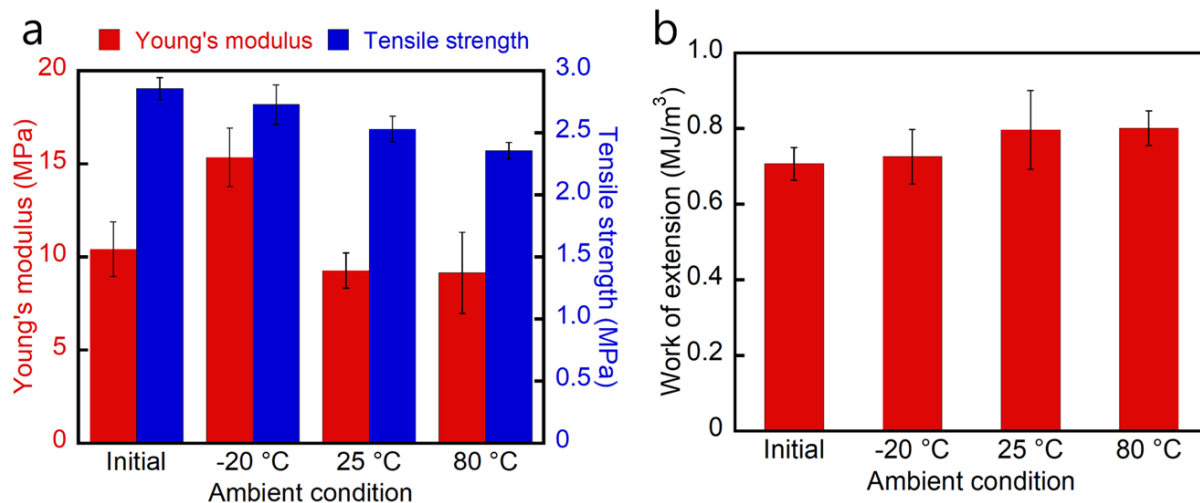
Supplementary Figure 9. (a) Compressive stress–strain curves of the cellulose/PVDF GGs and (b) corresponding Young’s moduli (left) and compressive strengths at 88% strain (right).



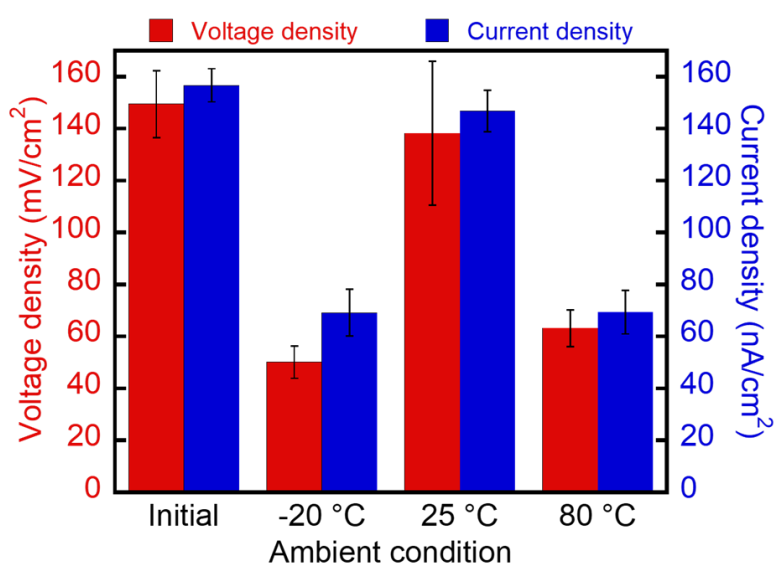
Supplementary Figure 10. Solvent contents of the cellulose/PVDF GGs.



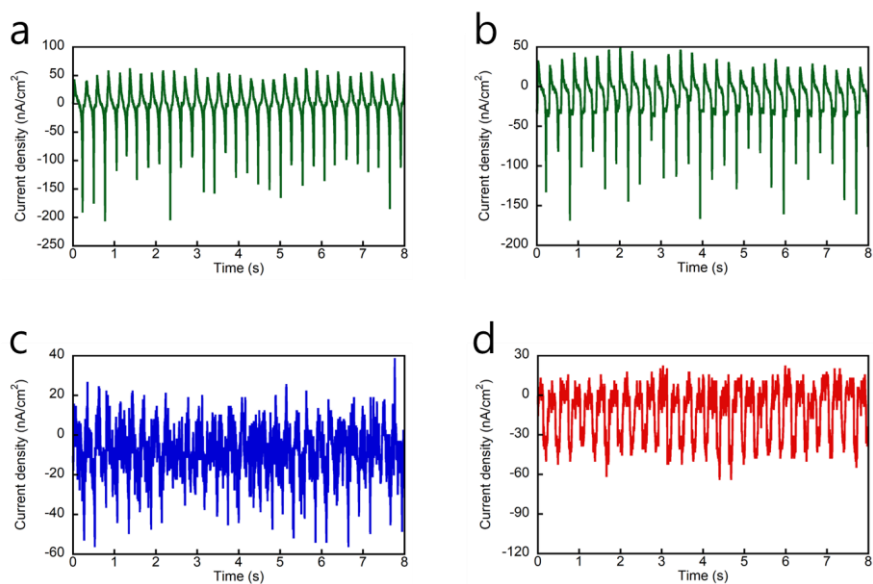
Supplementary Figure 11. Tensile loading–unloading curves of the (1/2)% cellulose/PVDF GG after different waiting times.



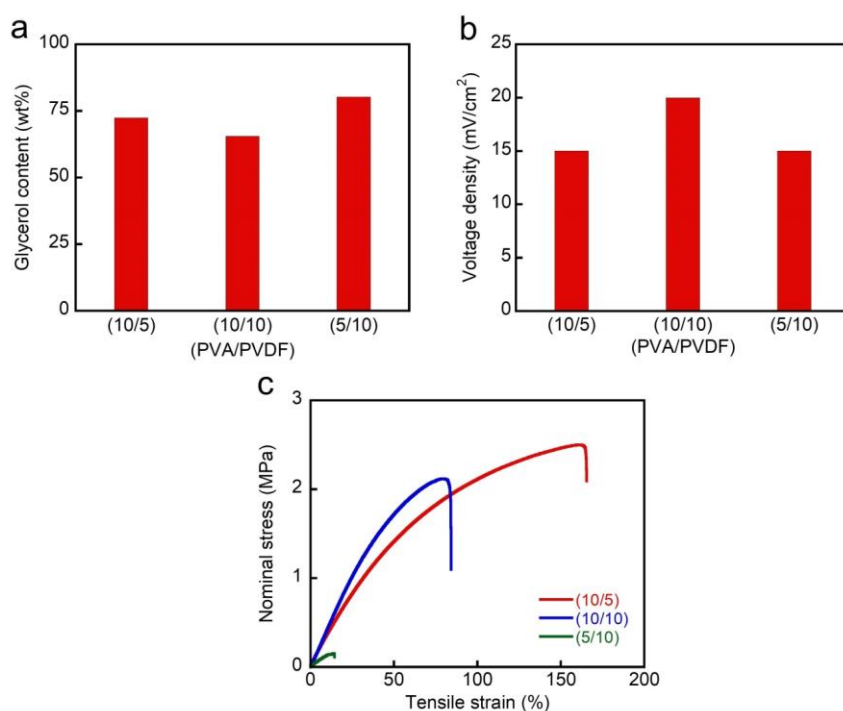
Supplementary Figure 12. (a) Young's moduli (left) and tensile strengths (right) and (b) work of extension of the (1/2)% cellulose/PVDF GG before and after 7 d of exposure to air at -20, 25, and 80 °C.



Supplementary Figure 13. Piezoelectric output voltages and current densities of the (1/2)% cellulose/PVDF GG subjected to finger-tapping loads before and after 7 d of exposure to air at -20, 25, and 80 °C.



Supplementary Figure 14. Output current densities of the (1/2)% cellulose/PVDF GG (a) before and (b–d) after 7 d of exposure to air at (b) -20 , (c) 25 , and (d) 80 °C (measured with respect to time under finger-tapping loads).



Supplementary Figure 15. (a) Glycerol content, (b) output voltage density, and (c) tensile stress–strain curves of ≈ 2 -mm-thick PVA/PVDF GGs with various polymer compositions.

Supplementary Table 1. Preparation of cellulose/PVDF solutions for GG synthesis.

Sample	Cellulose (g)	PVDF (g)	DMAc/LiCl (92/8) (w/w) solution (g)
1% Cellulose	0.5	0	49.5
(1.0/0.5)% Cellulose/PVDF	0.5	0.25	49.25
(1.0/1.0)% Cellulose/PVDF	0.5	0.5	49
(1.0/1.5)% Cellulose/PVDF	0.5	0.75	48.75
(1.0/2.0)% Cellulose/PVDF	0.5	1.0	48.5
(1.0/2.5)% Cellulose/PVDF	0.5	1.25	48.25
(1.0/3.0)% Cellulose/PVDF	0.5	1.5	48
(0.5/1.0)% Cellulose/PVDF	0.25	0.5	49.25
(0.5/1.5)% Cellulose/PVDF	0.25	0.75	49
(0.5/2.0)% Cellulose/PVDF	0.25	1.0	48.75
(0.5/2.5)% Cellulose/PVDF	0.25	1.25	48.5
(0.5/5.0)% Cellulose/PVDF	0.25	2.5	47.25
(1.5/1.0)%	0.75	0.5	48.75

Cellulose/PVDF			
(1.5/1.5)%	0.75	0.75	48.5
Cellulose/PVDF			
(1.5/2.0)%	0.75	1.0	48.25
Cellulose/PVDF			
(1.5/2.5)%	0.75	1.25	48
Cellulose/PVDF			

Supplementary Table 2. Piezoelectric response, tensile modulus, and working temperature of the proposed gel and similar existing gels.

Gel	Gel type	Output voltage	Tensile modulus (MPa)	Working temperature range (°C)	Reference
PAAm/PVDF	Hydrogel	2 mV cm ⁻²	No data	No data	[S1]
PAAm/PANI	Hydrogel	47 mV	No data	No data	[S2]
PAAm/PVDF-HFP/LiTFSI/PC	Hydrogel	22.5 mV cm ⁻²	No data	No data	[S3]
PAN/PVDF	Hydrogel	30 mV	4.24	No data	[S4]
PHEMA/GO	Hydrogel	15.24	0.253	No data	[S5]
PVA/PVDF/Ag nanowires	Hydrogel	360 mV	0.703	No data	[S6]
CHACC/PEDOT:PSS/PVDF-TrFE	Hydrogel	100 mV	0.2	No data	[S7]
Cellulose/PVDF	Glycerogel	363.33 ± 13.32 mV 1 (86.06 ± 6 mV cm ⁻²)	10.42 ± 1.47	-20 to 80	Present study

PAAm: poly(acryl amide)

PVDF: poly(vinylidene fluoride)

PANI: polyaniline

PVDF-HFP: poly(vinylidene fluoride-co-hexafluoropropylene)

LiTFSI: lithium bis(trifluoromethanesulfonyl) imide

PC: propylene carbonate

PAN: polyacrylonitrile

PHEMA: poly(2-hydroxyethyl methacrylate)

GO: graphene oxide

PVA: poly(vinyl alcohol)

CHACC: cross-linked chitosan quaternary ammonium salt

PEDOT:PSS: poly(3,4-ethylenedioxythiophene):poly(styrenesulfonate)

PVDF-TrFE: poly(vinylidene fluoride-co-trifluoroethylene)

Supplementary Movie 1. Piezoelectric output voltage of the (1/2)% cellulose/PVDF GG after incubation at $-20\text{ }^{\circ}\text{C}$ for 7 d.

Supplementary Movie 2. Piezoelectric output voltage of the (1/2)% cellulose/PVDF GG after incubation at $25\text{ }^{\circ}\text{C}$ for 7 d.

Supplementary Movie 3. Piezoelectric output voltage of the (1/2)% cellulose/PVDF GG after incubation at $80\text{ }^{\circ}\text{C}$ for 7 d.

Measurement and characterization procedures

Solvent content measurements

The glycerol contents of the gels were determined by calculating the difference between their initial and dried weights (W_0 and W_d , respectively). After its W_0 value was recorded, each gel was immersed in water for 1 d at 25 °C to replace glycerol with water. Water was changed several times to ensure that glycerol was completely substituted in the gel network. The resulting gel was completely dried at 120 °C for 1 d, and the W_d value was recorded. The solvent content was calculated using Eq. (S1).

$$\text{Solvent content (wt\%)} = \frac{W_0 - W_d}{W_0} \times 100\%. \quad (\text{S1})$$

Mechanical characterization

Tensile tests: For the tensile fracture and tensile loading–unloading tests, ~2-mm-thick gel samples were cut into rectangular shapes with lengths and widths of ~30 and ~3 mm, respectively. These specimens were clamped along the longitudinal direction in a tensile testing machine with a distance of ~10 mm between the two clamps. Tests were conducted by moving the upper clamp, which was connected to a 10 kgf load cell, upward. Tensile fracture and loading–unloading tests were performed at deformation rates of 500% min⁻¹ (0.083 s⁻¹) and 100% min⁻¹ (0.017 s⁻¹), respectively. Prior to the tests, the rectangular specimens were placed in temperature-controlled chambers for 7 d to evaluate their extremotolerant mechanical properties. Subsequently, the samples were removed from the chambers and immediately mounted on a tensile testing machine. Each type of gel was tested three times under each set of conditions. The tensile stress–strain curves were linearly fit over a strain range of 0.5%–1.0% to determine Young’s moduli. All data are presented as mean values with standard deviations.

Compression tests: Disk-shaped samples (diameter = 6 mm, thickness = ~2 mm) were subjected to compression tests. Each specimen was placed between two parallel steel plates, and the upper plate—which was connected to a 100 kgf load cell—was moved downward to apply a compressive load. Gels with different PVDF compositions were tested at a deformation rate of 20% min⁻¹ (0.0033 s⁻¹), and their extremotolerant mechanical properties were assessed at a deformation rate of 500% min⁻¹ (0.083 s⁻¹). Compressive loading–unloading tests were performed at a deformation rate of ~830% min⁻¹ (0.277 mm s⁻¹), which corresponded to the tapping speed in the piezoelectric output response tests. Each gel type

was tested three times under each set of conditions. The compressive stress–strain curves were linearly fit over a strain range of 0%–10% to obtain Young’s moduli. All data are presented as mean values with standard deviations.

Dielectric property characterization

The dielectric constants and dielectric losses of the gels were calculated using EIS data [S8]. The gel specimens (length × width × thickness: 20 mm × 20 mm × 2 mm) were sandwiched between two parallel stainless-steel electrodes and connected to a potentiogalvanostat in a two-electrode configuration. EIS was performed in the frequency range of 100–10⁵ Hz at an amplitude (V_{RMS}) of 10 mV. The dielectric constant (ϵ') and dielectric loss ($\tan \delta$) were calculated from complex impedance data using Eqs. (S3) and (S5):

$$\omega = 2\pi f, \quad (S2)$$

$$\epsilon' = \frac{t}{\omega A \epsilon_0} \cdot \frac{z''}{z'^2 + z''^2}, \quad (S3)$$

$$\epsilon'' = \frac{t}{\omega A \epsilon_0} \cdot \frac{z'}{z'^2 + z''^2}, \quad (S4)$$

$$\tan \delta = \frac{\epsilon''}{\epsilon'}, \quad (S5)$$

where f (Hz) is the applied frequency, ω is the angular frequency, t (m) is the specimen thickness, A (m²) is the cross-sectional surface area of the electrodes, ϵ_0 is the permittivity of free space (8.854×10^{-12} C² N⁻¹ m⁻²), z' (Ω) is the real part of the impedance, and z'' (Ω) is the imaginary part of the impedance.

Supplementary references

[S1] Islam, S.; Park, M.; Song, S. H.; Kim, A. Hydrogel-fractal piezoelectric bilayer transducer for wireless biochemical sensing. *In 42nd Annual International Conference of the IEEE Engineering in Medicine and Biology Society (EMBC)*, Montreal, QC, Canada, July 20–24, 2020, pp. 4089–92. DOI: 10.1109/EMBC44109.2020.9175819

[S2] Li, S.; Tao, Y.; Maryum, P.; *et al.* Bifunctional polyaniline electroconductive hydrogels with applications in supercapacitor and wearable strain sensors. *J Biomater Sci, Polym Ed* **2020**, *31*, 938–53. DOI: 10.1080/09205063.2020.1731787

[S3] Dobashi, Y.; Yao, D.; Petel, Y.; *et al.* Piezoionic mechanoreceptors: Force-induced current generation in hydrogels. *Science* **2022**, *376*, 502–507. DOI: 10.1126/science.aaw1974

[S4] Fu, R.; Tu, L.; Zhou, Y.; *et al.* A tough and self-powered hydrogel for artificial skin. *Chem Mater* **2019**, *31*, 9850–60. DOI: 10.1021/acs.chemmater.9b04041

- [S5] Zhao, W.; Shi, Z.; Hu, S.; Yang, G.; Tian, H. Understanding piezoelectric characteristics of PHEMA-based hydrogel nanocomposites as soft self-powered electronics. *Adv Compos Hybrid Mater* **2018**, *1*, 320–331. DOI: 10.1007/s42114-018-0036-3
- [S6] Wu, J.; Chen, T.; Wang, Y.; *et al.* Piezoelectric effect of antibacterial biomimetic hydrogel promotes osteochondral defect repair. *Biomedicines* **2022**, *10*, 1165. DOI: 10.3390/biomedicines10051165
- [S7] Hu, Z.; Li, J.; Wei, X.; *et al.* Enhancing strain-sensing properties of the conductive hydrogel by introducing PVDF-TrFE. *ACS Appl Mater Interfaces* **2022**, *14*, 45853–45868. DOI: 10.1021/acsami.2c13074
- [S8] Joshi, J. H.; Kanchan, D. K.; Joshi, M. J.; Jethva, H. O.; Parikh, K. D. Dielectric relaxation, complex impedance and modulus spectroscopic studies of mix phase rod like cobalt sulfide nanoparticles. *Mater Res Bull* **2017**, *93*, 63–73. DOI: 10.1016/j.materresbull.2017.04.013